Expedited Trust-Region-Based Design Closure of Antennas by Variable-Resolution EM Simulations

Slawomir Koziel[1,2][0000-0002-9063-2647], Anna Pietrenko-Dabrowska[2][0000-0003-2319-6782], and Leifur Leifsson[3][0000-0001-5134-870X]

[1] Engineering Optimization & Modeling Center, School of Science and Engineering, Reykjavík University, Menntavegur 1, 101 Reykjavík, Iceland
koziel@ru.is
[2] Faculty of Electronics Telecommunications and Informatics, Gdansk University of Technology, Narutowicza 11/12, 80-233 Gdansk, Poland
anna.dabrowska@pg.edu.pl
[3] Department of Aerospace Engineering, Iowa State University, Ames, IA 50011, USA
leifur@iastate.edu

Abstract. The observed growth in the complexity of modern antenna topologies fostered a widespread employment of numerical optimization methods as the primary tools for final adjustment of the system parameters. This is mainly caused by insufficiency of traditional design closure approaches, largely based on parameter sweeping. Reliable evaluation of complex antenna structures requires full-wave electromagnetic (EM) analysis. Yet, EM-driven parametric optimization is, more often than not, extremely costly, especially when global search is involved, e.g., performed with population-based metaheuristic algorithms. Over the years, numerous methods of lowering these expenditures have been proposed. Among these, the methods exploiting variable-fidelity simulations started gaining certain popularity. Still, such frameworks are predominantly restricted to two levels of fidelity, referred to as coarse and fine models. This paper introduces a reduced-cost trust-region gradient-based algorithm involving variable-resolution simulations, in which the fidelity of EM analysis is selected from a continuous spectrum of admissible levels. The algorithm is launched with the coarsest discretization level of the antenna under design. As the optimization process converges, for reliability reasons, the model fidelity is increased to reach the highest level at the final stage. The proposed algorithm allows for a significant reduction of the computational cost (up to sixty percent with respect to the reference trust-region algorithm) without compromising the design quality, which is corroborated by thorough numerical experiments involving four broadband antenna structures.

Keywords: Antenna design; EM-driven optimization; gradient search, variable-resolution simulations; model management.

1 Introduction

The use of full-wave electromagnetic (EM) simulations have become a commonplace in the design of modern antenna structures. This is primarily because EM analysis

ICCS Camera Ready Version 2021
To cite this paper please use the final published version:
DOI: 10.1007/978-3-030-77970-2_8

is the only tool capable of rendering reliable evaluation of increasingly complex designs, as well as accounting for mutual coupling effects, or the presence of environmental components (e.g., connectors) or nearby devices. In recent years, the emergence and rapid development of new application areas, e.g., the internet of things (IoT) [1], 5G wireless communications [2], wearable [3] or implantable devices [4], increased the complexity of antenna topologies even further. Such intricate designs, described by large numbers of optimizable variables, can no longer be tuned by means of supervised parameter sweeping. This enforces the employment of numerical optimization algorithms for antenna parameter refinement. Still, EM-driven optimization is unavoidably associated with high computational expenditures, which may turn unacceptable. Even the cost of the local gradient search [5], [6] may be sizeable. As far as global optimization is concerned, the number of required EM simulations required by the optimizer to converge may exceed several thousand [7], which significantly hinders applicability of popular procedures such as differential evolution [8], [9] evolutionary algorithms [10], [11], or particle swarm optimizers [12], [13].

A considerable research effort has been directed towards mitigation of the forenamed issues. One distinguishable group of techniques are algorithmic enhancements, in which gradient-based procedures are sped up by dedicated mechanisms. These include sparse Jacobian updates based on design relocation monitoring [14], sensitivity variation tracking [15], the employment of updating formulas [16], or a combination thereof [17]. Another option is the incorporation of adjoint sensitivities [18]. An entirely different approach is offered by surrogate-assisted frameworks, where a fast representation of the system at hand (referred to as a surrogate or a metamodel) replaces expensive EM simulations when making predictions about possibly improved parameter sets. The surrogates may be data-driven (e.g., kriging [19], radial basis functions [20], Gausssian process regression [21], or neural networks [22], to name but a few), or physics-based [23]. Nevertheless, in antenna design, the practical usage of data-driven models is hampered to a large extent by the curse of dimensionality, as well as significant nonlinearity of antenna characteristics. In consequence, the verification case studies reported in available literature typically feature two to just six adjustable parameters [24], [25].

Physics-based models may not be as popular as data-driven ones, still, they seem to be an attractive alternative in situations, where setting up the latter is hardly possible. Physics-based models incorporate the problem-specific knowledge in the form of low-fidelity representations of the system at hand, e.g., equivalent circuits [26], or coarse-mesh EM simulations [27]. To construct the surrogate, the low-fidelity model undergoes a correction (or enhancement) using a relatively small number of high-fidelity data samples. Popular optimization methods incorporating physics-based surrogates include space mapping [28], adaptive response scaling [29], and feature-based technology [30].

Computational efficiency of the optimization procedures may be enhanced by the employment of variable-fidelity simulations. In practice, however, two levels of model discretization are typically used. This paper introduces a novel optimization framework involving variable-resolution EM simulations embedded into the trust-region gradient search algorithm. The discretization levels are selected from the predefined spectrum, ranging from the lowest fidelity (still of a practical utility) to that ensuring sufficiently accurate representation of the antenna characteristics. The specific fidelity level is decided upon based on the optimization process convergence status, as well as the im-

ICCS Camera Ready Version 2021
To cite this paper please use the final published version:
DOI: 10.1007/978-3-030-77970-2_8

provement of the objective function value in the consecutive iterations. At the beginning of the entire process, the coarsest discretization level is adopted, which enables a relatively cheap exploitation of the knowledge about the antenna under study, and expedited exploration of the parameter space. The reliability of the design process is ensured by gradually increasing the model fidelity, eventually reaching the finest assumed resolution. Our methodology is demonstrated using a benchmark set of four broadband antennas, all optimized to improve their impedance matching. The efficacy of the approach is compared to the standard trust-region procedure, and several state-of-the art accelerated techniques. The computational savings are around sixty percent with respect to the reference, without significantly deteriorating the design quality.

2 Antenna Design by Variable-Resolution EM Simulations

This section delineates the proposed optimization framework exploiting variable-resolution simulations, in which the model fidelity is adjusted based on the convergence status of the optimization process. In the initial stage of our procedure, the antenna discretization density is set to the lowest value from the predefined spectrum of admissible levels. Next, it is gradually increased as the optimization process converges. The section is organised as follows. The antenna optimization task is formulated in Section 2.1. Section 2.2 provides a brief description of the conventional trust-region algorithm with numerical derivatives. The description of variable-resolution simulation models (Section 2.3), as well as the overall optimization framework (Section 2.4) concludes the section.

2.1 Simulation-Driven Antenna Design

Design closure refers to the stage of the antenna development process in which its topology has been already established, and the geometry parameters ensuring the best achievable performance are to be identified. This tuning requires a definition of a suitable metric quantifying the design quality. Toward this end, we employ a merit function $U(\boldsymbol{x})$, where $\boldsymbol{x}$ refers to the vector of antenna designable parameters. The optimization task is formulated as

$$\boldsymbol{x}^* = \arg\min_{\boldsymbol{x}} U(\boldsymbol{x}) \tag{1}$$

subject to the inequality $g_k(\boldsymbol{x}) \le 0$, $k = 1, \ldots, n_g$, and equality constraints $h_k(\boldsymbol{x}) = 0$, $k = 1, \ldots, n_h$. The definition of the objective function U reflects the design goals so that its lower values correspond to better designs. Here, we are interested in minimizing the antenna in-band reflection. Hence, the adopted merit function takes the following form $U(\boldsymbol{x}) = S(\boldsymbol{x}) = \max\{f \in F : |S_{11}(\boldsymbol{x},f)|\}$, where f denotes a frequency from the intended antenna operating range, and S_{11} denotes the (complex) reflection coefficient. As evaluation of the constraints corresponding to antenna electrical and/or field properties involves full-wave simulation, handling them explicitly is not straightforward. A convenient way of dealing with them is offered by a penalty function approach [31], where the design closure task is reformulated as follows:

$$\boldsymbol{x}^* = \arg\min_{\boldsymbol{x}} U_P(\boldsymbol{x}),\ U_P(\boldsymbol{x}) = U(\boldsymbol{x}) + \sum_{k=1}^{n_g+n_h} \beta_k c_k(\boldsymbol{x}) \tag{2}$$

In (2), U_P is a sum of the original merit function U and the penalty terms. The violation of each constraint is quantified by the factor $c_k(\boldsymbol{x})$, with β_k being the penalty coefficients.

ICCS Camera Ready Version 2021
To cite this paper please use the final published version:
DOI: 10.1007/978-3-030-77970-2_8

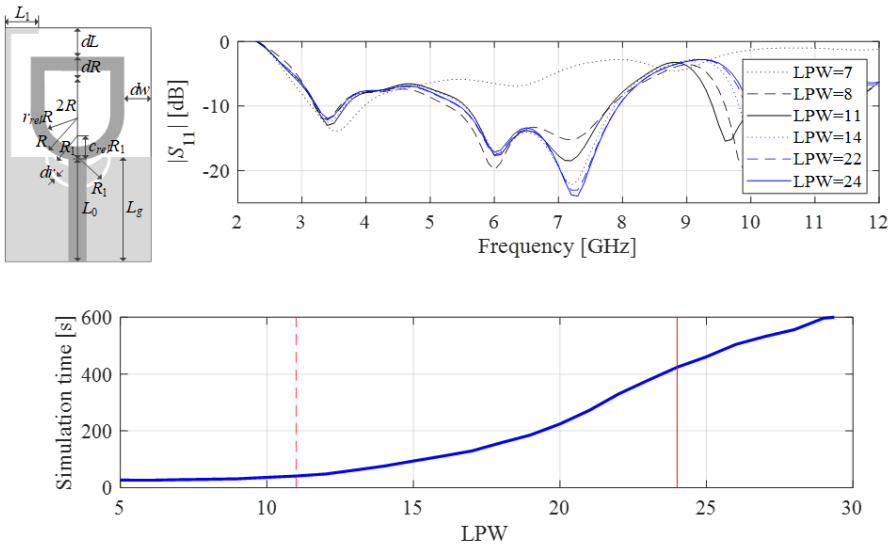

Fig. 1. Variable-resolution simulations: (a) a broadband monopole antenna; (b) the family of the antenna reflection responses simulated at various discretization levels (parametrized using the LPW parameter); (c) the dependence of the simulation time on LPW (averaged over several designs). The high- (—) and the minimum usable low-fidelity model (- - -) mesh densities are marked with vertical lines.

2.2 Trust-Region Gradient-Based Search

The core of our framework is a conventional trust-region (TR) algorithm [32], which is briefly recollected below. The optimization problem (1) (or (2), if the penalty function approach is applied) is solved in a local sense. During this process a series of approximations $\boldsymbol{x}^{(i)}$, $i = 0,1, \ldots$, to the optimum solution $\boldsymbol{x}^*$ is yielded. Each consecutive approximation $\boldsymbol{x}^{(i)}$ of $\boldsymbol{x}^*$ is obtained by optimizing the linear expansion model $U_L^{(i)}$ of the relevant antenna characteristics at the current iteration point $\boldsymbol{x}^{(i)}$. Here, we consider the antenna reflection response S_{11}, therefore we have

$$S_L^{(i)}(\boldsymbol{x}, f) = S_{11}(\boldsymbol{x}^{(i)}, f) + \boldsymbol{G}_S(\boldsymbol{x}^{(i)}, f) \cdot (\boldsymbol{x} - \boldsymbol{x}^{(i)}) \tag{3}$$

In (3), the gradient of S_{11} at $\boldsymbol{x}^{(i)}$ is denoted as $\boldsymbol{G}_S(\boldsymbol{x}^{(i)},f)$. $U_L^{(i)}$ is defined similarly as U_P (except for $S_L^{(i)}(\boldsymbol{x})$ replacing S_{11}). Other types of responses (e.g., gain), are handled in a similar manner. The approximations to the optimum solution are rendered as:

$$\boldsymbol{x}^{(i+1)} = \arg \min_{\boldsymbol{x};\, -\boldsymbol{d}^{(i)} \le \boldsymbol{x} - \boldsymbol{x}^{(i)} \le \boldsymbol{d}^{(i)}} U_L^{(i)}(\boldsymbol{x}) \tag{4}$$

The gradient $\boldsymbol{G}_S$ is typically estimated through finite differentiation (FD) at the cost of n additional EM analyses, where n stands for the antenna parameter number. The sub-problem (6) is solved within the interval $[\boldsymbol{x}^{(i)} - \boldsymbol{d}^{(i)}, \boldsymbol{x}^{(i)} + \boldsymbol{d}^{(i)}]$, referred to as the trust region. Here, the initial size vector $\boldsymbol{d}^{(0)}$ is made proportional to the bounds on the design variables so as to avoid variable scaling, and to allow for similar treatment of variables of significantly different ranges. This is because the antenna geometry parameters may range from less than a millimeter in the case of gaps up to as much as tens of millimeters, when the dimensions of the ground plane are considered. The improvement in the

ICCS Camera Ready Version 2021
To cite this paper please use the final published version:
DOI: 10.1007/978-3-030-77970-2_8

objective function value for the candidate design found by (6) leads to its acceptance. Otherwise, the iteration is repeated with a reduced TR vector size [32].

The basic version of the TR algorithm requires performing full FD update of the antenna sensitivities in each algorithm iteration. Recently, several expedited variations of TR algorithm have been reported that employ sparse sensitivity updating schemes [14]-[16]. Each of these methods exploits a different mechanism allowing for omitting FD in certain cases, including a relative design relocation control [14], gradient changes monitoring [15], or selective Broyden updates [16]. The proposed procedure has been benchmarked against two of these methods, i.e., [14] and [16], along with the original TR algorithm with full-FD sensitivity update (see Section 3).

2.3 Variable-Resolution EM Simulations

In this work, the optimization process is accelerated by employing variable-resolution EM simulations. Variable-fidelity methods have been widely used for expediting the design of antenna structures [25], [29], [33]. Yet, they are typically limited to two surrogate levels: low- and high-fidelity models (or, in other words, coarse and fine ones). In antenna design, coarse models are most often based on coarse-mesh EM simulations [34], whereas in microwave engineering, equivalent circuits are frequently employed [35]. The coarse model, upon applying a suitable correction, is capable of rendering reliable predictions of the system output and can be used to find the approximate optimal solution of the fine model. Among the methods of this class, space mapping [25] and response correction techniques [36] may be listed as representative examples.

Reliability and computational efficiency of the variable-fidelity optimization framework strongly depend on the appropriate selection of underlying low-fidelity model [37]. Let us consider an example. The family of reflection characteristics simulated at several levels of antenna discretization for an ultra-wideband antenna is shown in Fig. 1. Here, the discretization level is parametrized with the use of the LPW (lines per wavelength), which is employed for mesh density control in CST Microwave Studio, the commercial software package used for antenna evaluation. Selecting too low LPW causes excessive discrepancies between the corresponding model response and that of the high-fidelity model, thereby, making the model unusable. Coarser discretization is advantageous from the point of view of computational savings, yet, it may lead to deterioration of the design quality. These factors have to be taken into consideration while adjusting suitable model discretization level.

Analysis of the antenna response family, such as that presented in Fig. 1(b), allows us to establish an admissible LPW range for the device under study: from L_{min} (corresponding to the coarsest, yet still practically useful discretization) up to L_{max} (ensuring accurate representation of the antenna output). We aim at expediting the optimization process by exploiting the simulation models from the said range $L_{min} \leq L \leq L_{max}$, thereby improving computational efficiency of the entire optimization process. The adopted model management scheme allowing for suitable adjustment of the discretization level has been described in Section 2.4.

2.4 Model Management Scheme

This section outlines the adopted model management scheme that governs the fidelity of the EM model throughout the optimization run based on its convergence status.

ICCS Camera Ready Version 2021
To cite this paper please use the final published version:
DOI: 10.1007/978-3-030-77970-2_8

The assumption is that the model resolution is set with the use of the sole parameter $L \in (L_{\min},L_{\max})$, where $L_{\min}$ and $L_{\max}$ refer to the lowest acceptable and the fine discretization level, respectively. In our approach, the decision making scheme has been developed to satisfy the following requirements. For computational efficiency reasons, the optimization process should be initialized with the lowest admissible discretization level, thereby allowing for inexpensive exploitation of the problem-specific knowledge when searching for a better design. Whereas for reliability reasons, the last stages of the optimization procedure should be carried out at the highest discretization level. The intermediate discretization levels should be adjusted based on the algorithm convergence status: (i) $\|\boldsymbol{x}^{(i+1)} - \boldsymbol{x}^{(i)}\|$ (convergence in argument), and (ii) $U_P(\boldsymbol{x}^{(i+1)}) - U_P(\boldsymbol{x}^{(i)})$ (objective function improvement). To improve the stability of the optimization process, the transition between consecutive discretization levels should be as smooth as possible regarding the assumptions mentioned above.

In addition, the following algorithm termination conditions are applied (the algorithm terminates if either of them is satisfied): (i) $\|\boldsymbol{x}^{(i+1)} - \boldsymbol{x}^{(i)}\| < \varepsilon_x$; (ii) $\|\boldsymbol{d}^{(i)}\| < \varepsilon_x$; and (iii) $|U_P(\boldsymbol{x}^{(i+1)}) - U_P(\boldsymbol{x}^{(i)})| < \varepsilon_U$. In the numerical experiments of Section 3, the aforementioned thresholds are set to $\varepsilon_x = \varepsilon_x = 10^{-3}$. We also define an auxiliary variable

$$Q^{(i)}(\varepsilon_x,\varepsilon_U) = \max\left\{\frac{\varepsilon_x}{\|\boldsymbol{x}^{(i+1)} - \boldsymbol{x}^{(i)}\|}, \frac{\varepsilon_U}{|U_P(\boldsymbol{x}^{(i+1)}) - U_P(\boldsymbol{x}^{(i)})|}\right\} \tag{5}$$

The proposed convergence-based model management scheme works as follows: in the ith iteration, the discretization parameter $L^{(i)}$ is adjusted according to the following rule (which ensures discretization parameter monotonicity)

$$L^{(i+1)} = \begin{cases} L_{\min} & \text{if} \quad Q^{(i)}(\varepsilon_x,\varepsilon_U) \le M \\ \max\left\{L^{(i)}, L_{\min} + \left(L_{\max} - L_{\min}\right)\left[Q^{(i)}(\varepsilon_x,\varepsilon_U) - M\right]^{-\frac{1}{\alpha}}\right\} & \end{cases} \tag{6}$$

In the numerical experiments of Section 3, we adopt $M = 10^{-2}$ and $\alpha = 3$. Therefore, the initial increase of parameter L is rather quick, and it is launched two decades before the algorithm convergence (in terms of the norm-wise distance between the consecutive iteration points). As the simulation time strongly depends on the parameter L, the former seems to be reasonable: it brings substantial computational savings at the beginning of the entire process without significant detriment to its accuracy.

In order to ensure that at the end of the optimization run the EM model is evaluated at the highest discretization level, a safeguard mechanism is implemented enforcing that $L^{(i+1)}$ ultimately reaches $L_{\max}$. This is because the sole use of the formula (6) does not ensure eventual switching to $L_{\max}$, e.g., in the case of unsuccessful iterations causing the TR size vector to get smaller than the termination threshold and premature termination of the algorithm. Upon algorithm termination the following condition is applied

$$\text{IF} \;\; L^{(i)} < L_{\max} \;\; \text{THEN} \; L^{(i+1)} = L_{\max} \;\; \text{AND} \;\; \boldsymbol{d}^{(i+1)} = M_d \boldsymbol{d}^{(i)} \frac{\varepsilon_x}{\|\boldsymbol{d}^{(i)}\|} \tag{7}$$

In our experiments, we adopt multiplication factor $M_d = 10$. Thus, the termination condition is bypassed by (9), and subsequent iterations are carried out with $L^{(i+1)} = L_{\max}$. Clearly, if the value $L_{\max}$ has been already reached, the above safeguard mechanism is not triggered.

ICCS Camera Ready Version 2021
To cite this paper please use the final published version:
DOI: 10.1007/978-3-030-77970-2_8

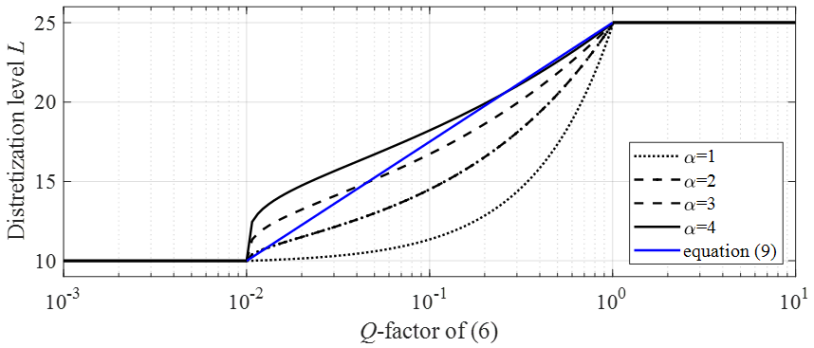

Fig. 2. Discretization level profiles for several values of the control parameter α (cf. (8)) along with a piece-wise profile (cf. (9). The plots have been created for $L_{\min} = 10$, $L_{\max} = 25$, and $M = 10^{-2}$.

Let us now discuss the selection of the control parameter α. Several profiles of the discretization levels for various values of α are shown in Fig. 2, and the additional piece-wise linear profile from $L_{\min}$ to $L_{\max}$ described by the parameter-less equation

$$L^{(i+1)} = \begin{cases} L_{\min} & \text{if } Q^{(i)}(\varepsilon_x, \varepsilon_U) \le M \\ \max\left\{ L^{(i)}, L_{\min} + \left(L_{\max} - L_{\min}\right)\left[1 - \dfrac{\log(Q^{(i)}(\varepsilon_x, \varepsilon_U)}{\log M}\right]\right\} \end{cases} \tag{8}$$

Observe that (10) is approximated most accurately by $\alpha = 3$ (which also more flexible). In our approach, in order to speed-up the optimization process, the evaluation of the antenna response sensitivities is carried out at a lower fidelity level assessed as $L_{FD} = \max\{L_{\min}, \lambda L^{(i)}\}$, where $0 \le \lambda \le 1$ is an algorithm control parameter (set to $\lambda = 2/3$ in numerical experiments of Section 3). This additional acceleration mechanism capitalizes on the fact that the models of different fidelities are typically well correlated even though they might be misaligned, and this correlation improves with an increase in $L^{(i)}$). This allows for rendering antenna response gradients in a reliable manner.

2.5 Optimization Framework with Variable-Resolution EM Simulations

The proposed optimization algorithm utilizes, as the search engine, the trust-region routine recollected in Section 2.2 in conjunction with the convergence-based model management scheme outlined in Section 2.4. The algorithm control parameters include: (i) ε_x, ε_U – termination thresholds; (ii) M – the threshold for launching discretization level increase; (iii) α – control parameter governing discretization level profile; (iv) λ – control parameter for L_{FD} adjustment (estimation of the antenna gradient); (v) M_d – multiplication factor serving to increase the TR size in (8), when closer to convergence.

The following general rules for setting the values of the aforementioned parameters apply. The termination thresholds ε_x and ε_U are to be set by the user so as to reflect the assumed resolution level of the optimization procedure. The remaining parameters are set to their default values $M = 10^{-2}$, $\alpha = 3$, $\lambda = 2/3$, and $M_d = 10$ (as elaborated on in Section 2.4). The extreme values $L_{\min}$ and $L_{\max}$ of the admissible spectrum of discretization levels (see Section 2.3) are to be selected by the user based on visual inspection

ICCS Camera Ready Version 2021
To cite this paper please use the final published version:
DOI: 10.1007/978-3-030-77970-2_8

of the family of antenna responses. $L_{\min}$ should be the lowest yet still practically useful discretization level, i.e., such that is capable of properly yielding all important details of the antenna response (e.g., its resonances). Whereas $L_{\max}$ should correspond to the high-fidelity model whose discretization level ensures sufficient accuracy.

3 Demonstration Examples

The benchmark set comprises four broadband antenna structures shown in Fig. 3. Table 1 provided the details concerning their parameter vectors (both designable and fixed ones), as well as the description of the substrate each structure is implemented on. All antennas are evaluated using the time-domain solver of CST Microwave Studio; all simulation models incorporate the SMA connectors. The intended operating frequency range is 3.1 GHz to 10.6 GHz. The design goal has been defined as minimization of the maximum in-band reflection within UWB band. The objective function is defined as $U(\boldsymbol{x}) = \max\{3.1\text{ GHz} \leq f \leq 10.6\text{ GHz} : |S_{11}(\boldsymbol{x},f)|\}$. Table 1 also gathers the ranges of the admissible values of lines-per-wavelength (LPW) parameter (see Section 2.3) for all antennas, along with the corresponding simulation times. The ranges are defined by $L_{\min}$ (the lowest practically usable discretrization), and $L_{\max}$ (the value for high-fidelity model).

The proposed optimization algorithm is benchmarked against the following three procedures: (i) the conventional TR algorithm [32] (Algorithm 1), (ii) the accelerated TR version [14] (Algorithm 2), in which sparse sensitivity updating scheme is based on relative design relocation, as well as (iii) the expedited version reported in [16] (Algorithm 3), employing the Broyden formula instead of FD for the selected variables. All benchmark procedures utilize solely high-fidelity EM simulations, i.e., the discretization level in each iteration equals $L^{(i)} = L_{\max}$ (for the respective antennas).

In Algorithm 2, proposed in [14], some of FD-based sensitivity updates are omitted for the variables that exhibit small relative change with respect to the current TR region size. In addition, the optimization history is monitored so that to ensure that the relevant portion of the sensitivity matrix is updated through FD once in few iterations. The algorithm control parameter N defines the maximum allowable number of update-free iterations. Here, the numerical results have been obtained for $N = 3$. For a more detailed account of Algorithm 2, see [14]. The acceleration mechanism of the Algorithm 3 consists in replacing FD a rank-one Broyden formula (BF) for the selected variables whose directions are aligned well enough with the most recent design relocation. The alignment threshold is the algorithm control parameter: as it increases, BF is applied less frequently, thereby, enforcing more frequent FD updates and possibly leads to design quality enhancement. More details on Algorithm 3 can be found in [16].

All the considered algorithms are the local procedures and, in general, the presented optimization tasks are multimodal. Therefore, carrying out the search from different initial designs typically yields distinct local optima. Multimodality is mainly caused by a parameter redundancy occurring for the considered antenna structures, which, in turn, is a result of the modifications introduced to their geometries aiming at size reduction.

The average performance of all the algorithms is assessed with the use of the following factors: (i) computational efficiency expressed in terms of the number of equivalent

ICCS Camera Ready Version 2021
To cite this paper please use the final published version:
DOI: 10.1007/978-3-030-77970-2_8

EM evaluations, (ii) design quality estimated as the average value of the objective function across the performed optimization runs, and (iii) result repeatability quantified by standard deviation of the objective function values across the entire set. As a consequence of the problem multimodality, the standard deviation is non-zero even for the reference TR algorithm (Algorithm 1), being presumably the most reliable procedure of the entire benchmark set. Therefore, the observed deterioration of the design repeatability should be compared with that of Algorithm 1.

Table 1. Verification structures

Antenna	Geometry parameters [mm]	Substrate	Lowest-fidel. model		High-fidelity model	
			L_{min}	Simulation time [s]	L_{min}	Simulation time [s]
I [38]	$\boldsymbol{x} = [l_0\ g\ a\ l_1\ l_2\ w_1\ o]^T$ $w_0 = 2o + a$, $w_f = 1.7$	RF-35: $\varepsilon_r = 3.5$ $h = 0.76$ mm	10	42	21	150
II [39]	$\boldsymbol{x} = [L_0\ dR\ R\ r_{rel}\ dL\ dw\ Lg\ L_1\ R_1\ dr\ c_{rel}]^T$ $w_0 = 1.7$	RF-35: $\varepsilon_r = 3.5$ $h = 0.76$ mm	11	41	24	424
III [40]	$\boldsymbol{x} = [L_g\ L_0\ L_s\ W_s\ d\ dL\ d_s\ dW_s\ dW\ a\ b]^T$ $W_0 = 3.0$	FR4: $\varepsilon_r = 4.3$ $h = 1.55$ mm	10	46	20	265
IV [41]	$\boldsymbol{x} = [L_0\ L_1\ L_2\ L\ dL\ L_g\ w_1\ w_2\ w\ dw\ L_s\ w_s\ c]^T$ $w_0 = 1.7$	RO4350: $\varepsilon_r = 3.48$ $h = 0.76$ mm	10	37	25	97

Table 2. Antenna I and II: Optimization results and benchmarking

Algorithm	Antenna I					Antenna II				
	Cost[1]	Cost savings[2]	max $\lvert S_{11}\rvert$[3]	Δ max $\lvert S_{11}\rvert$[4]	std max $\lvert S_{11}\rvert$[5]	Cost[1]	Cost savings[2]	max $\lvert S_{11}\rvert$[3]	Δ max $\lvert S_{11}\rvert$[4]	std max $\lvert S_{11}\rvert$[5]
1	97.6	–	–11.9	–	0.4	111.2	–	–14.9	–	0.6
2 [14]	45.1	53.8 %	–11.1	0.8	1.0	58.3	48%	–13.7	1.2	1.3
3 [16]	53.0	46 %	–10.7	1.2	2.7	75.9	32%	–14.3	0.6	1.0
This work	48.2	51 %	–11.2	0.7	0.7	25.8	77%	–13.8	1.1	1.0

[1] Number of equivalent high-fidelity EM simulations (averaged over 10 algorithm runs).
[2] Relative computational savings in percent w.r.t. the reference TR algorithm.
[3] Objective function value (maximum in-band reflection in dB), averaged over 10 algorithm runs.
[4] Degradation of max$\lvert S_{11}\rvert$ w.r.t. the reference algorithm in dB, averaged over 10 algorithm runs.
[5] Standard deviation of max$\lvert S_{11}\rvert$ in dB across the set of 10 algorithm runs.

Table 3. Antenna III and IV: Optimization results and benchmarking

Algorithm	Antenna III					Antenna IV				
	Cost[1]	Cost savings[2]	max $\lvert S_{11}\rvert$[3]	Δ max $\lvert S_{11}\rvert$[4]	std max $\lvert S_{11}\rvert$[5]	Cost[1]	Cost savings[2]	max $\lvert S_{11}\rvert$[3]	Δ max $\lvert S_{11}\rvert$[4]	std max $\lvert S_{11}\rvert$[5]
1	111.0	–	–13.9	–	1.0	139.7	–	–17.6	–	1.2
2 [14]	73.1	34 %	–12.8	1.1	1.3	91.2	34 %	–16.3	1.3	2.5
3 [16]	80.0	28 %	–11.9	1.9	2.0	89.2	36 %	–15.1	2.5	2.6
This work	42.3	62 %	–11.3	2.6	1.0	97.2	31 %	–17.0	0.6	2.1

[1] Number of equivalent high-fidelity EM simulations (averaged over 10 algorithm runs).
[2] Relative computational savings in percent w.r.t. the reference TR algorithm.
[3] Objective function value (maximum in-band reflection in dB), averaged over 10 algorithm runs.
[4] Degradation of max$\lvert S_{11}\rvert$ w.r.t. the reference algorithm in dB, averaged over 10 algorithm runs.
[5] Standard deviation of max$\lvert S_{11}\rvert$ in dB across the set of 10 algorithm runs.

ICCS Camera Ready Version 2021
To cite this paper please use the final published version:
DOI: 10.1007/978-3-030-77970-2_8

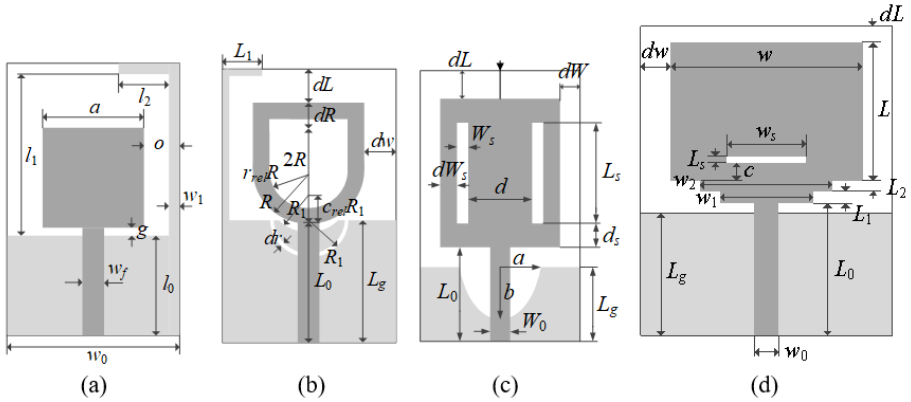

Fig. 3. Broadband antennas: (a) Antenna I, (b) Antenna II, (c) Antenna III, (d) Antenna IV. Light gray shade indicates ground plane.

The values of the control parameters of the proposed procedure have been set to (see also Section 2.4): $M = 10^{-2}$ (discretization level increase threshold), $\alpha = 3$ (control parameter for adjusting discretization level profile), $\lambda = 2/3$ (FD discretization level L_{FD} control parameter), $M_d = 10$ (multiplication factor for increasing the TR size when closer to convergence). For all the algorithms, the following termination thresholds $\varepsilon_x = \varepsilon_U = 10^{-3}$ have been adopted.

The numerical results for Antennas I through IV have been obtained for ten independent algorithm runs starting from random initial designs, and gathered in Tables 2 and 3, respectively. The Tables include the optimization cost calculated as the equivalent number of high-fidelity antenna evaluations, the cost savings w.r.t. the reference TR algorithm, as well as the objective function value, its deterioration w.r.t. Algorithm 1 and the standard deviation. The comparison of the latter should take into account the value obtained for the conventional algorithm. The cost of the proposed algorithm employing variable-resolution EM simulations is computed based on the time evaluation ratios between the low- and the high-fidelity models. Figure 4 presents the selected reflection characteristics for the initial and optimized designs.

The results indicate that the proposed optimization framework outperforms the benchmark routines in terms of the computational efficiency for all the considered antenna structures. The average speedup exceeds 55 percent (from around 30 percent for Antenna IV up to almost 80 percent for Antenna II). The cost savings are comparable to that of the expedited versions [14] and [16] using solely high-fidelity simulations (in the case of Antennas I and IV), or are even considerably higher (in the case of Antennas II and III). This is a consequence of the evaluation ratios between the high- and lowest-fidelity models, which are larger for Antennas I and IV (10.3 and 5.8, respectively), and smaller for Antennas II and III (3.6 and 2.6, respectively). This implies that the computational efficiency of the proposed procedure will likely benefit from expanding the discretization level range. Actually, here, the maximum admissible discretization level $L_{\max}$ does not coincide with the high-fidelity model. It has been merely treated as such for the sake of consistency with the results provided in [14] and [16]. Setting larger values of $L_{\max}$ would likely result in reaching further computational speedup.

ICCS Camera Ready Version 2021
To cite this paper please use the final published version:
DOI: 10.1007/978-3-030-77970-2_8

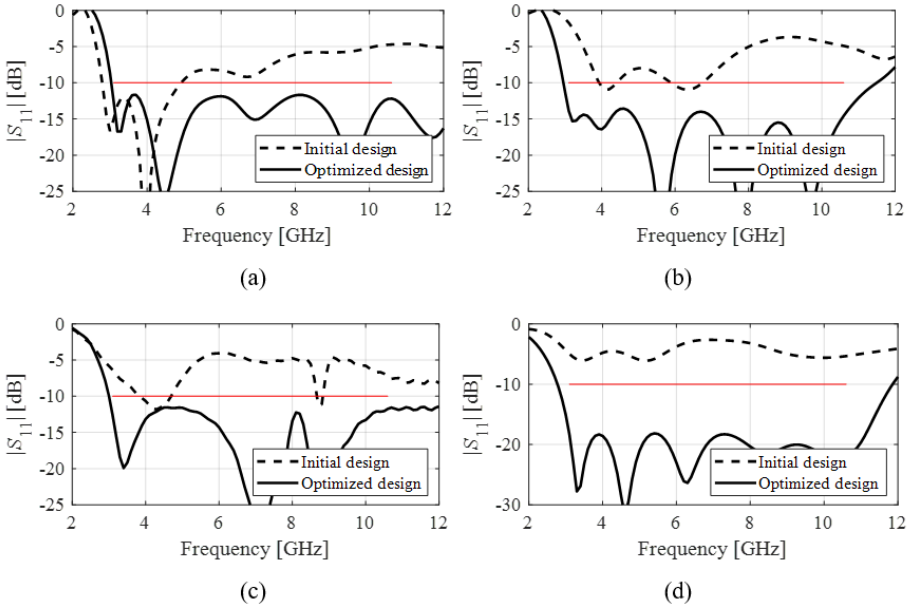

Fig. 4. Initial (- - -) and optimized (—) reflection responses of the benchmark antennas at the selected designs obtained using the proposed multi-fidelity framework: (a) Antenna I, (b) Antenna II, (c) Antenna III, (d) Antenna IV. Horizontal lines idicate design specifications.

As far as the design quality degradation is concerned, the proposed algorithm performs similarly or even better than the accelerated procedures [14] or [16] (except for Antenna III). In our approach, the average deterioration of the design quality is minor, not exceeding 1 dB. Additionally, the obtained standard deviation values (describing the solution repeatability) is similar to that of the reference TR procedure.

4 Conclusion

In the paper, a novel trust-region-based algorithm with variable-resolution EM simulation for expedited optimization of antenna structures has been proposed. Our approach exploits a decision making routine, in which model fidelity is continuously adjusted based on the optimization convergence status. The algorithm is initiated with lowest (least expensive) admissible level of model discretization. In the subsequent iterations, the model resolution is gradually increased. The model of the highest fidelity is utilized only as the algorithm gets closer to the optimum, in order to ensure reliability of the entire process. This allows for achieving a significant computational speedup of around eighty percent (in comparison to the conventional trust-region routine) owing to a low-cost exploitation of the problem-specific knowledge embedded in models of lower discretization levels at early stages of the optimization run. Our methodology has been comprehensively validated using the benchmark set comprising four broadband antennas. The proposed framework also outperforms the recently reported accelerated trust-region-based routines exploiting sparse sensitivity updates in terms of the design

ICCS Camera Ready Version 2021
To cite this paper please use the final published version:
DOI: 10.1007/978-3-030-77970-2_8

quality. At the same time, the computational efficiency is comparable or even better. The future work will include introducing acceleration mechanisms similar to those employed in the benchmark techniques, which will possibly result in additional computational speedup.

Acknowledgement

The authors would like to thank Dassault Systemes, France, for making CST Microwave Studio available. This work was supported in part by the Icelandic Centre for Research (RANNIS) Grant 217771 and by National Science Centre of Poland Grant 2017/27/B/ST7/00563.

References

1. Jha, K.R., Bukhari, B., Singh, C., Mishra, G., Sharma, S.K.: Compact planar multistandard MIMO antenna for IoT applications. IEEE Trans. Ant. Prop. vol. **66**(7), 3327–3336 (2018)
2. Nie, Z. Zhai, H., Liu, L., Li, J., Hu, D., Shi J.: A dual-polarized frequency-reconfigurable low-profile antenna with harmonic suppression for 5G application. IEEE Ant. Wireless Prop. Lett. **18**(6), 1228–1232 (2019)
3. Yan, S., Soh, P.J., Vandenbosch, G.A.E.: Wearable dual-band magneto-electric dipole antenna for WBAN/WLAN applications. IEEE Trans. Ant. Prop. **63**(9), 4165–4169 (2015)
4. Wang, J., Leach, M., Lim, E.G., Wang, Z., Pei, R., Huang, Y.: An implantable and conformal antenna for wireless capsule endoscopy. IEEE Ant. Wireless Prop. Lett. **17**(7), 1153–1157 (2018)
5. Ohira, M., Miura, A., Taromaru, M., Ueba, M.: Efficient gain optimization techniques for azimuth beam/null steering of inverted-F multiport parasitic array radiator (MuPAR) antenna. IEEE Trans. Ant. Prop. **60**(3), 1352–1361 (2012)
6. Wang, J., Yang, X.S., Wang, B.Z.: Efficient gradient-based optimization of pixel antenna with large-scale connections. IET Microwaves Ant. Prop. **12**(3), 385–389 (2018)
7. Lalbakhsh, A., Afzal, M.U., Esselle, K.: Multiobjective particle swarm optimization to design a time-delay equalizer metasurface for an electromagnetic band-gap resonator antenna. IEEE Ant. Wireless Propag. Lett. **16**, 912–915 (2017)
8. Goudos, S.K., Siakavara, K., Vafiadis, E., Sahalos, J.N.: Pareto optimal Yagi-Uda antenna design using multi-objective differential evolution. Progress In Electromagnetics Research. **105**, 231–251 (2010)
9. Zaharis, Z.D., Gravas, I.P., Lazaridis, P.I., Glover, I.A., Antonopoulos, C.S., Xenos, T.D.: Optimal LTE-protected LPDA design for DVB-T reception using particle swarm optimization with velocity mutation. IEEE Trans. Ant. Prop. **66**(8), 3926–3935 (2018)
10. Oliveira, P.S., D'Assunção, A.G., Souza, E.A.M., Peixeiro, C.: A fast and accurate technique for FSS and antenna designs based on the social spider optimization algorithm. Microw. Opt. Technol. Lett. **58**, 1912–1917 (2016)
11. Haupt, R.L.: Antenna design with a mixed integer genetic algorithm. IEEE Trans. Ant. Prop. **55**(3), 577–582 (2007)
12. Lalbakhsh, A., Afzal, M.U., Esselle, K.P., Smith S.L.: Wideband near-field correction of a Fabry-Perot resonator antenna. IEEE Trans. Ant. Propag. **67**(3), 1975–1980 (2019)

ICCS Camera Ready Version 2021
To cite this paper please use the final published version:
DOI: 10.1007/978-3-030-77970-2_8

13. Zaharis, Z.D., Gravas, I.P., Yioultsis, T.V., Lazaridis, P.I., Glover, I.A., Skeberis, C., Xenos, T.D.: Exponential log-periodic antenna design using improved particle swarm optimization with velocity mutation. IEEE Trans. Magnetics. **53**(6), 1–4 (2017)

14. Koziel, S., Pietrenko-Dabrowska, A.: Reduced-cost EM-driven optimization of antenna structures by means of trust-region gradient-search with sparse Jacobian updates. IET Microwaves, Ant. Prop. **13**(10), 1646–1652 (2019)

15. Koziel, S., Pietrenko-Dabrowska, A.: Expedited feature-based quasi-global optimization of multi-band antennas with Jacobian variability tracking. IEEE Access. **8**, 83907–83915 (2020)

16. Koziel, S., Pietrenko-Dabrowska, A.: Expedited optimization of antenna input characteristics with adaptive Broyden updates. Eng. Comp. **37**(3), 851–862 (2019)

17. Koziel, S., Pietrenko-Dabrowska, A.: Reduced-cost design closure of antennas by means of gradient search with restricted sensitivity updates. Metrology Meas. Systems, **26**(4), 595–605 (2019)

18. Koziel, S., Ogurtsov, S., Cheng, Q.S., Bandler, J.W.: Rapid EM-based microwave design optimization exploiting shape-preserving response prediction and adjoint sensitivities. IET Microwaves, Ant. Prop. **8**(10), 775–781 (2014)

19. Hassan, A.K.S.O., Etman, A.S., Soliman, E.A.: Optimization of a novel nano antenna with two radiation modes using kriging surrogate models. IEEE Photonic J. **10**(4), 4800807 (2018)

20. Barmuta, P., Ferranti, F., Gibiino, G.P., Lewandowski, A., Schreurs, D.M.M.P.: Compact behavioral models of nonlinear active devices using response surface methodology. IEEE Trans. Microwave Theory Techn. **63**(1), 56–64 (2015)

21. Jacobs, J.P.: Characterization by Gaussian processes of finite substrate size effects on gain patterns of microstrip antennas. IET Microwaves Ant. Prop. **10**(11), 1189–1195 (2016)

22. Rawat, Yadav, R.N., Shrivastava, S.C.: Neural network applications in smart antenna arrays: a review. AEU - Int. J. Elec. Comm. **66**(11), 903–912 (2012)

23. Toktas, A., Ustun, D., Tekbas, M.: Multi-objective design of multi-layer radar absorber using surrogate-based optimization. IEEE Trans. Microw. Theory Techn. **67**(8), 3318–3329 (2019)

24. Lv, Z., Wang, L., Han, Z., Zhao, J., Wang, W.: Surrogate-assisted particle swarm optimization algorithm with Pareto active learning for expensive multi-objective optimization. IEEE/CAA J. Automatica Sinica. **6**(3), 838–849 (2019)

25. Cervantes-González, J.C., Rayas-Sánchez, J.R., López, C.A., Camacho-Pérez, J.R., Brito-Brito, Z., Chávez-Hurtado, J.L.: Space mapping optimization of handset antennas considering EM effects of mobile phone components and human body. Int. J. RF Microwave CAE. **26**(2), 121–128 (2016)

26. Bandler, J.W., Cheng, Q.S., Dakroury, S.A., Mohamed, A.S., Bakr, M.H., Madsen, K., Sondergaard, J.: Space mapping: the state of the art. IEEE Trans. Microwave Theory Techn. **52**(1), 337–361 (2004)

27. Koziel, S., Ogurtsov, S.: Antenna Design by Simulation-Driven Optimization. Surrogate-Based Approach. Springer, New York (2014)

28. Feng, F., Zhang, J., Zhang, W., Zhao, Z., Jin, J., Zhang, Q.J.: Coarse- and fine-mesh space mapping for EM optimization incorporating mesh deformation. IEEE Microwave Wireless Comp. Lett. **29**(8), 510–512 (2019)

ICCS Camera Ready Version 2021
To cite this paper please use the final published version:
DOI: 10.1007/978-3-030-77970-2_8

29. Koziel, S., Unnsteinsson, S.D.: Expedited design closure of antennas by means of trust-region-based adaptive response scaling. IEEE Antennas Wirel. Propag. Lett. **17**(6), 1099–1103 (2018)

30. Koziel, S.: Fast simulation-driven antenna design using response-feature surrogates. Int. J. RF & Microwave CAE. **25**(5), 394–402 (2015)

31. Ullah, U., Koziel, S., Mabrouk, I.B.: Rapid re-design and bandwidth/size trade-offs for compact wideband circular polarization antennas using inverse surrogates and fast EM-based parameter tuning. IEEE Trans. Ant. Prop. **68**(1) 81–89 (2019)

32. Conn, A.R., Gould, N.I.M., Toint, P.L.: Trust Region Methods, MPS-SIAM Series on Optimization (2000)

33. Su, Y., Li, J., Fan, Z., Chen, R.: Shaping optimization of double reflector antenna based on manifold mapping. Int. Applied Comp. Electromagnetics Soc. Symp. (ACES). Suzhou, China, 1–2 (2017)

34. Bandler, J.W., Cheng, Q.S., Dakroury, S.A., Mohamed, A.S., Bakr, M.H., Madsen, K., Sondergaard, J.: Space mapping: the state of the art. IEEE Trans. Microwave Theory Tech. **52**(1), 337–361 (2004)

35. Koziel, S., Ogurtsov, S.: Antenna Design by Simulation-Driven Optimization. Surrogate-Based Approach, Springer, New York (2014)

36. Koziel, S., Unnsteinsson, S.D.: Expedited design closure of antennas by means of trust-region-based adaptive response scaling. IEEE Antennas Wireless Prop. Lett., **17**(6), 1099–1103 (2018)

37. Koziel, S., Ogurtsov, S.: Model management for cost-efficient surrogate-based optimization of antennas using variable-fidelity electromagnetic simulations. IET Microwaves Ant. Prop. **6**(15), 1643–1650 (2012)

38. Koziel, S., Bekasiewicz, A.: Low-cost multi-objective optimization of antennas using Pareto front exploration and response features. Int. Symp. Antennas Prop., Fajardo, Puerto Rico (2016)

39. Alsath, M.G.N., Kanagasabai, M.: Compact UWB monopole antenna for automotive communications. IEEE Trans. Ant. Prop. **63**(9), 4204–4208 (2015)

40. Haq, M.A., Koziel, S.: Simulation-based optimization for rigorous assessment of ground plane modifications in compact UWB antenna design. Int. J. RF Microwave CAE. **28**(4), e21204 (2018)

41. Suryawanshi, D.R., Singh, B.A. A compact UWB rectangular slotted monopole antenna. IEEE Int. Conf. Control, Instrumentation, Comm. Comp. Tech. (ICCICCT), 1130–1136 (2014)

ICCS Camera Ready Version 2021
To cite this paper please use the final published version:
DOI: 10.1007/978-3-030-77970-2_8